Morphology, optical, and electric properties of polymerquantum dots nanocomposites: effect of polymeric matrix

I. Moura [1,*], A. de Sá [1], Ana S. Abreu [1], M. Oliveira [1], and A. V. Machado [1]

[1] Institute of Polymers and Composites (IPC) and Institute of Nanostructures, Nanomodelling and Nanofabrication (i3N), University of Minho, Campus de Azurém, 4800-058 Guimarães, Portugal

Abstract

Polymer-CdTe quantum dots (QDs) nanocomposites were developed via solvent casting. Colloidal CdTe QDs, synthesized in aqueous solution, were transferred to organic media by exchanging of the original capping ligands by a long-chain thiol. Different commercial polymers (PMMA, OPS, PS, and PC), transparent in the visible spectral range, were chosen as matrices. Stock solutions of the polymers were prepared in suitable concentration (2wt%) for the production of thin films with good quality, able to maximize the solubility of QDs, without phase separation. Studies on the morphological and optical properties were performed. The results showed that the polymer matrix has a considerable effect on QDs' morphology, size, and electric conductivity. PMMA demonstrated to be the most promising embedding matrix, offering new possibilities for optoelectronic applications of polymer-QD nanocomposites.

Introduction

Colloidal semiconductor nanoparticles (NPs), socalled quantum dots (QDs), with a diameter ranging from 1 to 50 nm , exhibit unique optical and electrical properties, that prompt them as good candidates to replace conventional semiconductor materials and organic dyes [1]. Particularly, cadmium tellurium (CdTe) QDs, due to their exceptional optical properties, dependent on their size and type of stabilizing ligand, exhibit a strong quantum confinement and are high-efficient photoluminescent materials, with exceptional physicochemical properties [2].

For their application in the nanotechnology field, such as in photovoltaic devices and light-emitting diodes (LEDs), QDs should be immobilized in a solid support or embedded in a soft matter matrix. Polymers are suitable materials for this purpose, since they are cheap, can be transparent, flexible, and easily processed [3]. Thus, research efforts have been made to combine the optical properties of QDs with the optical/mechanical/processing properties of polymers [4, 5]. In the development of films and other micro/nanostructures for practical applications, it is crucial to keep the individual properties of QDs, by preventing their agglomeration and photoluminescence quenching [1].

Nevertheless, it is difficult to induce high dispersion of QDs in a polymer matrix due to their incompatibility with organic solvents and polymers. Therefore, it is hard to keep the inter-particle distance between QDs that is crucial to determine their quantum yield (Φ_f), i.e., the optical properties of the resulting materials [6, 7] and produce polymer-QD nanocomposites as efficient materials, with novel optical, electrical, and mechanical properties [8, 9].

The use of capping ligands for nanoparticles modification, and subsequent stabilization, allows the preparation of polymer-QD nanocomposites that preserve the original nanoparticles' properties [10]. However, the nature of the capping ligand can significantly influence their compatibility with the bulk polymer, since phase separation of the QDs can originate agglomerates or even larger clusters in the polymer [10, 11].

CdTe QDs are generally synthetized in aqueous medium and stabilized with an appropriate organic ligand, the short-chain thioglycolic acid (TGA) [12, 13]. However, for optoelectronic applications, a compatibility between polymers and common organic solvents with the QDs capping ligands is required, preventing the use of water-soluble QDs. Therefore, it is necessary to adopt strategies that allow to transfer water-synthesized QDs to organic solvents, without compromising their high photoluminescence [14].

Several studies have been focused on the incorporation of water-soluble CdTe QDs into polymer matrices in order to produce materials with interesting properties. Water-soluble CdTe QDs have been mixed with hydrophilic polymers, such as poly(vinyl alcohol) (PVA) and poly (vinyl pyrrolidone) (PVP), producing polymer-QD nanocomposites that retain the optical efficiency of the NPs [9]. In other study [15], a surfactant, octadecyl- p-vinyl-benzyldimethylammonium chloride (OVDAC), was used to transfer aqueous CdTe into organic phases and subsequently produce CdTe -polystyrene (PS) and CdTe-PS/poly (methyl methacrylate) (PMMA) nanocomposites. The same procedure was applied to mix these NPs with lipophilic poly(α-methylstyrene) (PMS) and polycarbonate (PC) [9]. High-transparent CdTe-PMMA nanocomposites were developed using a polymerizable surfactant to link the NPs' surface ligands to the polymer matrix, avoiding agglomeration and preserving transparency [16]. Another approach used in the preparation of QDs-PMMA nanocomposites was based on dispersing QDs, capped with trioctylphosphine oxide (TOPO), into methyl methacrylate (MMA) solutions and promoting the radical polymerization of the monomers into PMMA [17]. This approach leads to the formation of a promising material for optoelectronic applications. Ananthakumar et al. [18] reported the use of CdTe QDs capped with 1-dodecanethiol (1-DDT) for the preparation of P3HT nanofibers. The resulting material showed effective interaction of the NPs with the polymer's structure. Most of the studies reported in the literature have been focused on the research of new methodologies to modify QDs to be embedded into polymers by simply mixing both materials. Only a few studies have been devoted to understand the size and structural evolution of QDs in the resulting nanocomposites [19, 20], and how the chemical interaction between the capping ligands and the polymers can influence the charge transport within the nanocomposites [21].

The present work is focused on studying the effect of the polymer matrix on morphology, optical, and electrical properties of polymer-QDs nanocomposites. CdTe-DDT QDs, due to their optoelectronic properties were chosen to prepare the nanocomposites. Several conventional lipophilic polymers, including polystyrene (PS), oxazoline functionalized polystyrene (OPS), poly(methyl methacrylate) (PMMA), and polycarbonate (PC), were selected based on their optical transparency in the visible spectral range and excellent processability, as polymeric matrices. Thin films of the nanocomposite materials were obtained by solvent casting. Homogeneous, nonporous, and transparent films were obtained by controlling the solvent evaporation (time and temperature). The morphology and charge transport efficiency of the prepared materials were characterized.

Materials and methods

materials

Tellurium powder (200 mesh, 99.99 %) and cadmium chloride anhydrous ($CdCl_2$, 99.99 %) were purchased to Alfa Aesar. Sodium borohydride ($NaBH_4$, 98%) and chloroform-d($CDCl_3$, $\geq$ 99.9%) were supplied by Acros Organics. Thioglycolic acid (TGA, 97 %), chloroform (99.9 %), and acetone (99.9 %) were acquired to Fisher Chemical. 1-dodecanethiol (1-DDT, $\geq$ 98%) was purchased to Sigma-Aldrich. Polystyrene (PS, Solarene G116, MFI 2.3 $g/10$ min at 200 $^{\circ}C$ with 5 kg), oxazoline functionalized polystyrene (OPS, Epocros RPS-1005, 6 $-$ 10 $g/10$ min at 200$^{\circ}C$ with 5 kg), poly(methyl methacrylate) (PMMA, Altuglas VSE UVT, MFI 27 $g/10$ min at 230$^{\circ}C$ with 3.8 kg), polycarbonate (PC, SABIC, LEXAN ^{TM} Resin 101) were used as polymeric matrices. Milli-Q ultrapure water was used in the synthesis of the nanoparticles. All the chemicals were used as received.

Preparation of sodium hydrogen telluride (NaHTe)

An aqueous solution of NaHTe was prepared based on the reported method for a NaHSe solution [22], with some modifications. Tellurium powder (0.119 g, 0.935 mmol) and $NaBH_4$ (0.082 g, 2.17mmol) were loaded into a Schlenk tube. The air was replaced with N_2. Then, ultrapure water (20 mL), under N_2 atmosphere, was added using a syringe. The mixture was stirred, at 80$^{\circ}C$, with continuous N_2 flow, until a deep red solution was obtained (45 min). NaHTe solution was used immediately after reaching room temperature.

Synthesis of TGA-coated CdTe quantum dots

CdTe-TGA QDs were synthesized according to a method previously reported in the literature [23], with minor modifications. Briefly, 0.037 g of $CdCl_2$ (0.202 mmol) was dissolved in ultrapure water (40 mL) and mixed with 0.035 mL of TGA (0.505 mmol), in a two-necked flask. The pH was adjusted to 10 by addition of 1 M NaOH . Then, the mixture was bubbled with N_2 atmosphere for 30 min .1 .8 mL of freshly prepared NaHTe solution was promptly added to the mixture, using a syringe, at room temperature. The final solution was stirred at $90^{\circ}C$, with continuous N_2 flow, during 6 h , in order to obtain CdTe-TGA QDs with the desired emission wavelength. The reaction was stopped by removing the heat source and cooling the reaction with an ice bath. Concentrate solutions of QDs were obtained after 20 min of centrifugation with 3500 rpm , using Amicon Ultra-15 centrifugal Filters (3000 MWCO).

Functionalization of quantum dots with 1dodecanethiol

High photoluminescent thiol-capped CdTe-TGA QDs, previously synthetized in aqueous solution, were subject to an exchange of the capping ligands. The experimental procedure was performed according to the strategy described elsewhere [14]. Briefly, 1 mL of 1-DDT was added on the top of 1 mL of an aqueous solution of CdTe-TGA nanoparticles, with a concentration within 10^{-3}M range, followed by the addition of 2 mL of acetone. The mixture was stirred and heated to the boiling point of acetone ($56^{\circ}C$). The transfer of the nanoparticles from the aqueous to the organic phase was detected by monitoring the color change of the latter. CdTe-DDT QDs were separated by decantation, diluted with toluene (1:1), and the nanoparticles precipitated with methanol.

Nanoparticles characterization

UV-Vis absorption spectra of QDs solutions were acquired on a Shimadzu UV3101PC UV-Vis-NIR spectrophotometer. The photoluminescence spectra (PL) were obtained, upon excitation at 360 nm , using a Microplate Reader Synergy MX (Bioteck Instruments). All the optical measurements were performed under ambient conditions. The photoluminescence quantum yield (Φ_f) of the QDs in solution, was estimated by comparing the integrated emission of the QDs samples, obtained at one excitation wavelength ($\lambda_{\text{exc}} = 360$ nm), with that of a standard photoluminescent dye, Rhodamine B, in ethanol $\left(\left[\left(\Phi_f\right) = 70\%\right]\right)$ [24]. Stock solutions of the standard and QDs samples, with similar absorbance (~ 0.022) at the same excitation wavelength, are assumed to absorb the same number of photons. Thus, a simple ratio of the integrated photoluminescence intensities of the standard and the QDs solutions provided the ratio of the quantum yield values. Identical instrument settings for the samples and standard solutions were used, and the solvent absorption and emission spectra were subtracted from the samples' absorption and emission spectra.

The morphology of the dispersed QDs was analyzed using transmission electron microscopy (TEM). For TEM analysis, the ultrasonically dispersed QDs were drop-casted over carbon-coated copper grids, dried, and the micrographs acquired with a JEOL JEM1010 microscope, operating at 100 kV .

Fourier transformed infrared spectroscopy (FTIR) spectra of the lyophilized CdTe-TGA and precipitated CdTe-DDT quantum dots were recorded with a Perkin-Elmer 1720 spectrometer. Measurements were performed in attenuated total reflectance mode (ATR) from 4000 to 500 cm^{-1}, after 32 scans with a resolution of 4 cm^{-1}. The vibrations were assigned based on reference tables published in literature [25].

Proton nuclear magnetic resonance (^{1}H NMR) spectra were acquired in a 400 MHz Avance Bruker NMR spectrometer equipped with an ultrashield magnet. A temperature of $25^{\circ}C$ and deuterated solvents, water (D_2O), and dimethylsulfoxide ($DMSOd_6$) were used in the analysis. The ^{1}H chemical shifts are reported in ppm (parts per million). The residual solvent peak has been used as an internal reference.

The QDs' zeta potential was measured, in solution, in order to evaluate the stability of colloidal dispersions, using dynamic light scattering (DLS) NANO ZS Malvern Zetasizer equipment (Worcestershire, UK), at $25^{\circ}C$, using a $He-Ne$ laser of 633 nm and a detector angle of 173°. Three independent measurements were performed for each sample. Malvern dispersion technology software (DTS) (Worcestershire, UK) was used with multiple narrow mode (high-resolution) data processing.

Thermogravimetric analysis of CdTe-TGA and CdTe-DDT solutions were carried out using a TA Q500 thermobalance. The samples were heated from 40 to $900^{\circ}C$ at $10^{\circ}C/min$ under nitrogen flow ($60\ mL/min$).

Production of nonporous thin films

Polymeric films with a thickness ranging from 2 to 6μ m were obtained by spreading a chloroform solution of each polymer ($2wt\%$) on the surface of flat polytetrafluoroethylene (PTFE). The complete solvent evaporation was performed both at room temperature, during the required time, and at $55^{\circ}C$ for 20 min . Subsequently, the films were removed from the PTFE substrate. Scanning electron microscopy (SEM) and scanning transmission electron microscopy (STEM), using a Leica Cambridge S360 microscope, were used to analyze the morphology and particles size.

Preparation of polymer-QDs nanocomposites

Polymer-QDs nanocomposites were produced by dispersing, by 1 h ultrasonication, at room
temperature, a CdTe-DDT QDs solution with a concentration around 10^{-3}M, in different polymeric matrices (PMMA, OPS, PS, and PC). The viscosity of the solutions was controlled by the ratio of the polymer and QDs solutions volume, corresponding to an amount of 2 and 13wt%, of polymer and QDs, respectively.

Thin films of the prepared materials were produced on PTFE substrates as aforementioned described.

Polymer-QDs nanocomposites characterization

The morphology of the dispersed QDs was analyzed by STEM and TEM, as described previously. Samples of 100 nm thickness were cut using a diamond knife, in a Leica ultra-microtome at $-40^{\circ}\mathrm{C}$. The cut sections were transferred to copper grids and then analyzed.

Atomic force microscopy (AFM) was performed in the tapping mode, using a Digital Instruments Multimode equipment controlled by Nanoscope III.

The emission spectra of the nanocomposites were recorded in a LabRAM HR Evolution spectrometer, equipped with a 532 nm laser (Laser Quantum Torus 532, power 50 to 750 mW) for excitation of the samples. 30 spectra (acquisition time: 10 s ; accumulations: 5; grating: $600\mathrm{gr/mm}$; ND filter: 25%; hole: 400), of a $10.88\ \mathrm{mm}^2 (2.98\mu\ \mathrm{m} \times 3.65\mu\ \mathrm{m})$ area afforded the Raman map of the studied area. An appropriate averaging procedure was applied afterwards.

The absorption spectra of the polymer-QDs nanocomposites were measured on a Shimadzu UV3101PC UV-Vis-NIR spectrophotometer.

Electrical properties of the thin films, produced at $55\ ^{\circ}\mathrm{C}$, were studied based on $I - V$ curves (where I is intensity and V is voltage) measured with an automated Keithley 487 picoammeter/voltage source, at room temperature. $I - V$ data points were collected between gold (Au) contacts, previously coated in a Polaron SC502 sputter coater. $I - V$ curves were obtained with an applied voltage ranging between -10 V and +10 V with 1 V gap, while measuring the current.

Results and discussion

Absorption and photoluminescence spectra of the CdTe-TGA and CdTe-DDT QDs are presented in Fig. 1. A strong band in the UV range, related to the

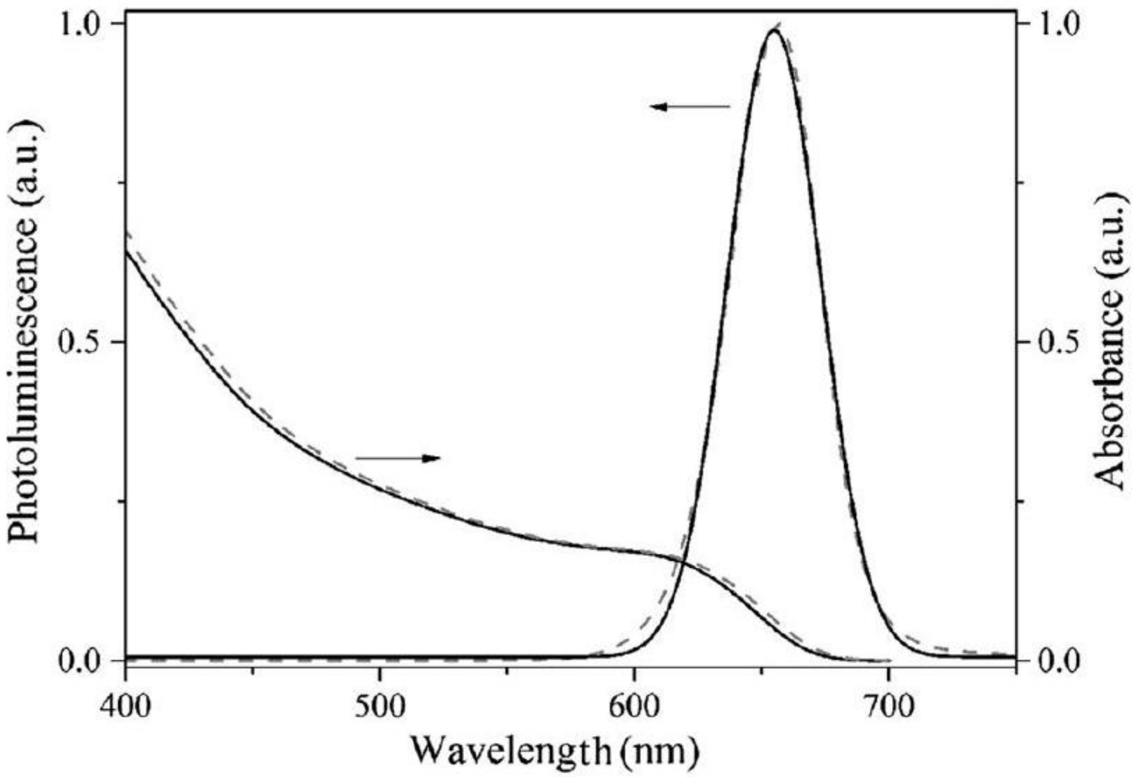

Figure 1 Normalized UV-Vis absorption and PL spectra of colloidal CdTe QDs before (solid lines) and after (dashed lines) phase transfer (from water to chloroform). lowest confined exciton state, with a long tail extending into the visible range, can be seen in both cases. The excitonic peak is centered approximately at 619 and 625 nm , for CdTe-TGA and CdTe-DDT, respectively, which is related with the QDs' size. The excitonic peak width is related to the size distribution and differences in QDs' morphology. The resulting CdTe-TGA's PL emission peak has a full width at half maximum (FWHM) of 40 nm , and is centered around 655 nm , Stokes-shifted with respect to the absorption peak, is associated to the exciton ground state in the QDs. CdTe QDs capped with 1-dodecanethiol evidenced a FWHM of 41 nm , and is centered at slightly higher wavelength (657 nm). The exchange of the capping ligand, TGA by 1-DDT, also reduced the photoluminescence quantum yield (Φ_f) from 52.5 to 36.0 %, which could be due to the formation of surface traps during the exchange of the capping agents, the extent of ligand exchange, and the chemical properties of the thiolate ligand [14]. Using an empirical relationship between the absorption wavelength of the first excitonic peak [26], it is possible to estimate the diameter of both QDs, 3.80 and 3.90 nm , respectively, for CdTe-TGA and CdTe-DDT. This slight difference is attributed to the red-shift of the emission spectra (Fig. 1), which is associated with the increase of the nanoparticles size.

TEM micrographs and size distributions of CdTe TGA and CdTe-DDT QDs are depicted in Fig. 2. It can be noticed that both CdTe QDs are well dispersed, with nearly spherical shape and without aggregation. Based on the peak maximum of a

Gaussian fitting, CdTe-TGA QDs have a diameter of 3.8 nm , in agreement with the results already discussed, while CdTe-DDT QDs have a slight higher diameter of 4.4 nm . It is clear in the histograms that the QDs have dissimilar size distributions, predominating the 4 nm NPs for both cases. While CdTe-TGA QDs have higher number of particles with 3 than 5 nm , for CdTe-DDT the number of NPs with 3 nm decreases considerably and NPs with 5 nm are present almost in the same amount as those with 4 nm . Morphological analyses evidence that the optical properties and size of the QDs were not significantly affected by replacing the capping ligand.

Additionally, TEM analysis of CdTe-DDT nanoparticles showed that, when transferred to chloroform, QDs have better spatial separation, which can be an explanation to the decrease of their Φ_f. Similar observation was reported by Gaponik et al. [14] regarding CdTe-TGA nanoparticles transferred into the organic phase after surface modification with 1-dodecanethiol. They attributed the differences in the spatial separation to the long-chain stabilizer, in comparison with thiol short chains. A similar study reported by Ananthakumar et al. [27] showed that after exchange, the water-soluble cadmium selenide (CdSe) nanoparticles' capping ligand, TGA by 1-DDT, a very good monodispersability of particle size distribution was achieved.

Besides the morphological characterization, the synthesized and phase-transferred nanoparticles were studied in terms of their structure and thermal stability. Thus, after the exchange of TGA by 1-DDT, $^{1}\mathrm{H}$ NMR spectroscopy was used to verify the presence of these ligands on the QDs' surface. The $^{1}\mathrm{H}$ NMR spectrum (data not shown) of CdTe-DDT QDs revealed NMR resonances that were in agreement with the presence of 1-dodecanethiol and none related to TGA, which confirmed a successful functionalization.

FTIR spectra of CdTe-TGA and CdTe-DDT QDs are given in Fig. 3. For CdTe-TGA QDs, the most pronounced FTIR absorption bands appear at $3700-3300\ \mathrm{cm}^{-1}$ and $1750-1600\ \mathrm{cm}^{-1}$, corresponding to hydroxyl (-OH) and carbonyl (-C=O) stretching vibrations, respectively. A weak peak appears in the range where -CH stretching vibrations of $\mathrm{CH_2}$ groups ($3000-2800\ \mathrm{cm}^{-1}$) are expected. Additionally, bands at $1240-1050\ \mathrm{cm}^{-1}$ and $750\ \mathrm{cm}^{-1}$ were assigned to $-\mathrm{C}-\mathrm{O}$ and $-\mathrm{C}-\mathrm{S}$ stretching vibrations, respectively. This proved that the QDs were capped

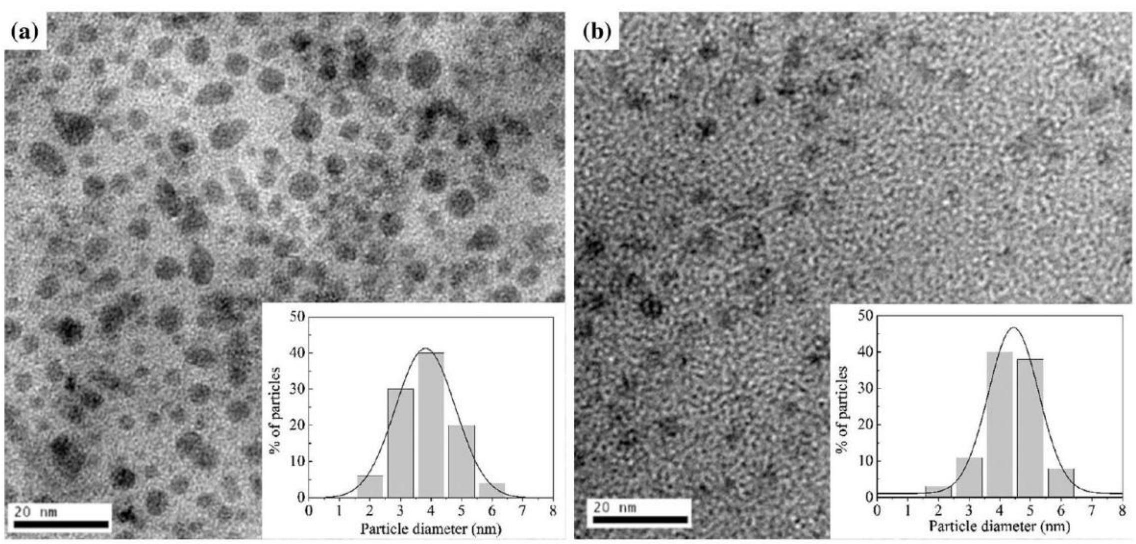

Figure 2 TEM micrographs and particle size histograms of the CdTe-TGA (a) and CdTe-DDT (b) QDs.

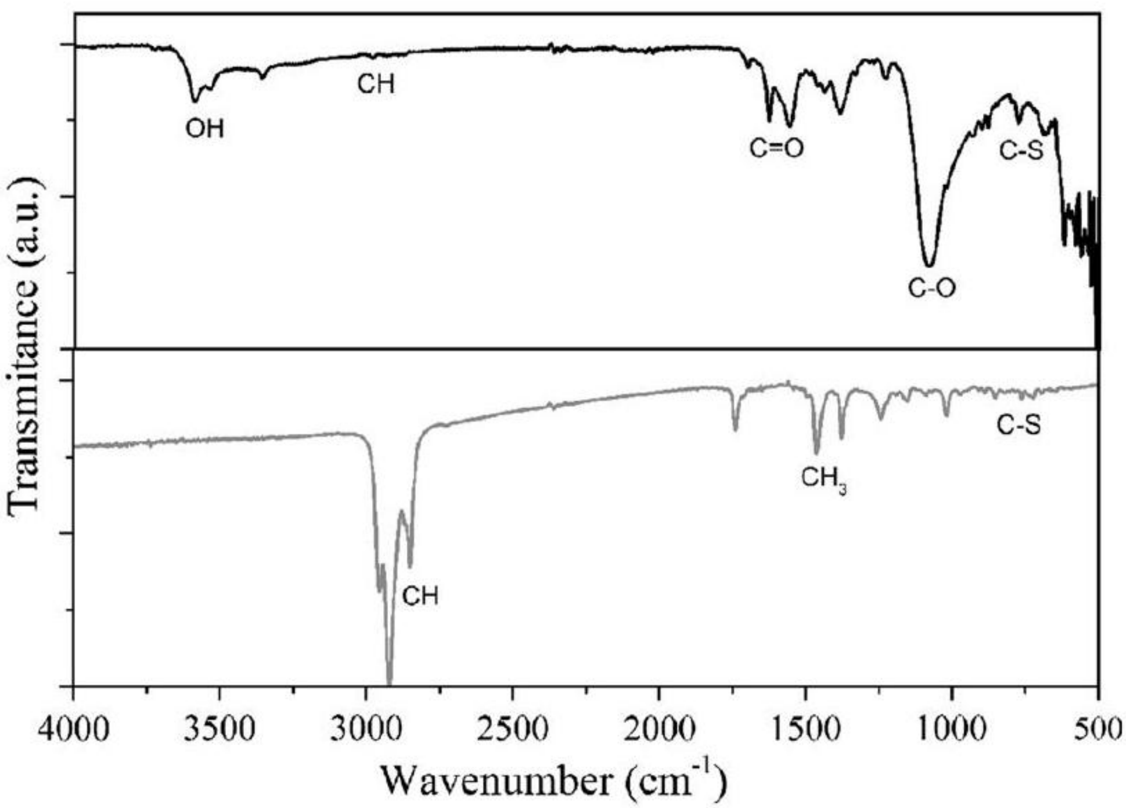

Figure 3 FTIR spectra of CdTe-TGA QDs (up) and CdTe-DDT (down). with TGA. After QDs' surface modification, the characteristic absorption bands of TGA disappeared. Additionally, it was observed that most of the characteristic bands of CdTe-DDT resemble those of pure 1-DDT, revealing that this long-chain thiol is indeed part of the material composition. The absorption band at $3000-2800\ \mathrm{cm}^{-1}$ was attributed to the -CH vibrations from 1-DDT, the vibration band at $1462\ \mathrm{cm}^{-1}$ was assigned to the asymmetrical CH_3 bending, the $1378\ \mathrm{cm}^{-1}$ band was attributed to the symmetrical CH_3 bending, and the weak peak at $750\ \mathrm{cm}^{-1}$ was assigned to $-\mathrm{C}-\mathrm{S}$ vibration. The absence of $-\mathrm{C}=\mathrm{O}$ and -OH stretching vibrations confirms that the ligand exchange reaction was successfully accomplished. In both spectra, the absence of -SH vibrations ($\sim 2570\ \mathrm{cm}^{-1}$), expected if the thiol groups are covalently bound to the surface of nanocrystals, corroborates the anchoring of TGA and 1-DDT molecules to the QDs' surface [10, 28].

Zeta potential measurements of TGA- and 1-DDTcapped CdTe QDs gave surface charge values of approximately -45 mV and +39.6 mV , respectively. These measurements confirm that, as expected, the surface of the nanoparticles is negative and positively charged, due to the chemical structure of the capping ligand. For colloidal QDs, it is generally known that their surface charge is mainly due to their capping ligands [28].

Figure 4 shows the thermogravimetric curves of CdTe-TGA and CdTe-DDT in the temperature range between 40 and $900^{\circ}\mathrm{C}$, to follow the ligand exchange process. The synthesized CdTe-TGA QDs contained a significant amount of TGA, as evidenced by the 75% weight loss, occurred along several degradation stages. The successful exchange of the original TGA ligands by 1-DDT was confirmed by the completely different thermal behavior of the material. The CdTeDDT QDs' thermogram indicates that the capping ligand degrades in two degradation stages, at 224 and

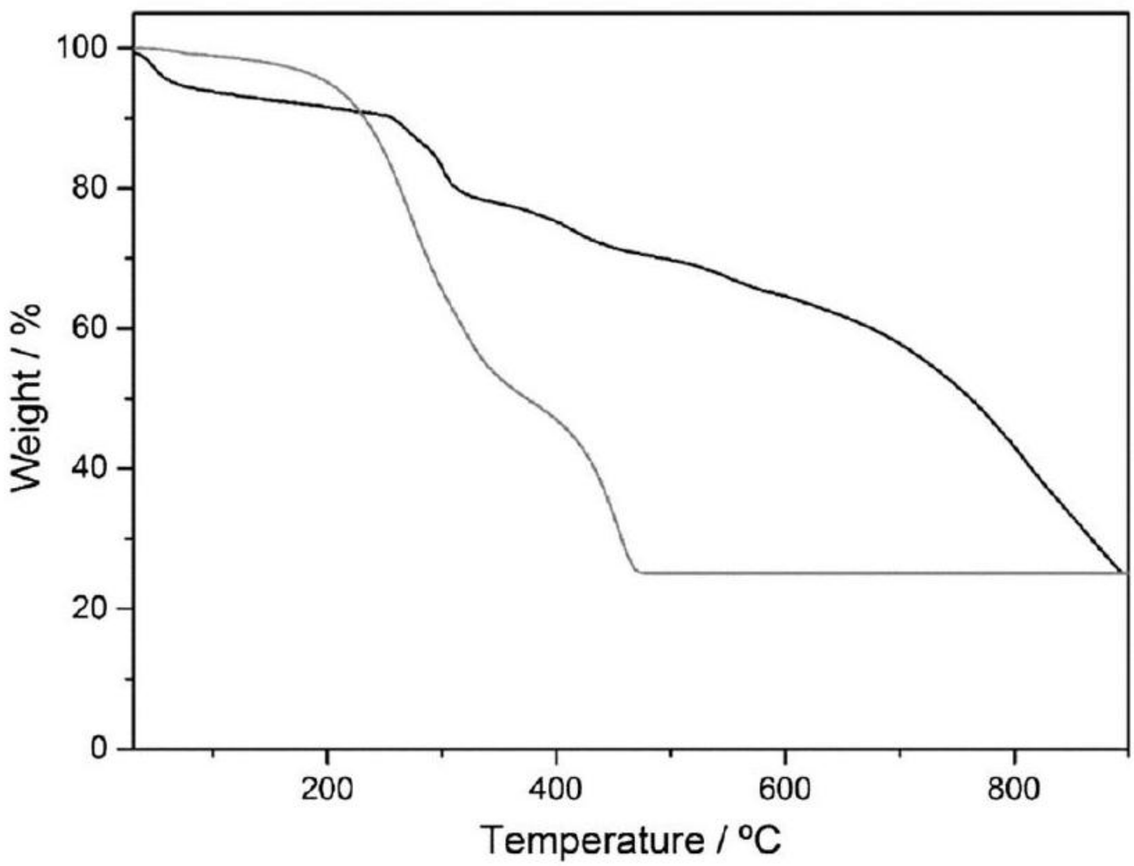

Figure 4 Thermogravimetric curves of CdTe-TGA (black line) and CdTe − DDT (gray line).
$428^{\circ}C$, corresponding to 76% of the material. The thermograms of both NPs show that, at $900^{\circ}C$, it still remain 25 and 24% of the initial material, respectively, for the TGA- and DDT-capped NPs, which correspond to the CdTe inorganic core.

Solvent evaporation rate is a key factor to avoid the formation of nonporous thin films [29]. Thus, the production of the polymer thin films was tested by solvent casting by promoting solvent evaporation both at room temperature and at $55^{\circ}C$ with different results. The slower solvent evaporation, at room temperature, lead to the formation of voids between PC's spherulites, observed by SEM and STEM (data not shown). These voids, also observed for PMMA, OPS, and PS, result in the productions of thin films with high degree of porosity. As a consequence, these films showed high opacity and fragility. Further, the porosity induces the degradation of the electrical properties of the resulting material, inhibiting the charge transport, which is essential for optoelectronic applications [29]. Additionally, the mechanical performance is also affected by the high porosity and the thin films and cannot be oriented by stretching, due to the high fragility. Films produced at higher evaporation rate, were transparent and homogeneous, crack-free, and without porosity, as it can be seen in Fig. 5. Therefore, after optimization, the processing conditions of PMMA, OPS, PS, and PC, the colloidal CdTe-DTT QDs were incorporated by direct mixing a QDs' solution with each polymer solution. PolymerQD nanocomposite films with thickness ranging from 2 to 6μ m were obtained.

Figure 6 depicts the STEM and TEM micrographs of polymer-QD nanocomposites prepared, which showed different QDs' morphologies, as the polymers' dissimilar chemical structures allowed to anticipate. When dispersed in PC, QDs tend to form larger aggregates. PC, with the higher T_g due to its backbone essentially composed by benzene rings, have low flexibility, thus limiting its capacity to accommodate the QDs within polymer chains. Although 1-DDT and the benzene rings could establish van der Waals (vdW) interactions, the latter, due to steric hindrance, are less available for such interactions. Thus, interaction between QDs particles is more favorable, promoting aggregation [9], resulting in the formation of clusters with diameter between 90 and 140 nm (Fig. 6a). PS has a chemical structure less rigid than PC that may facilitate the accommodation of the QDs. However, particle aggregates with diameters between 70 and 90 nm were found (Fig. 6c). This may be due to the fact that the vdW interaction between 1-DDT and the lateral benzyl groups is not sufficiently stronger to disrupt the π stacking in which the latter may be participating in. In the case of PMMA and OPS matrices, a better dispersion was observed, where clusters with diameter in the range of 40 to 60 nm were formed (Fig. 6b and d). PMMA has flexible small groups that do not establish strong interaction between them, facilitating the accommodation of the particles and allow them to easily establish interactions with the polymer chains, preventing aggregation. In the case of OPS, despite of being a PS derivative, the presence of oxazoline may cause empty volume in the polymer that can be occupied by the QDs, preventing aggregation. Additionally, it may cause such structural arrangements that the π-stacking is no longer so effective, thus allowing vdW interactions with 1-DDT. The TEM study was important to verify that, in the case of PMMA and OPS, the nanocomposites consist of inorganic nanoparticles surrounded by the polymer matrix, dispersed throughout the polymer domains, whereas for PC and PS, the inorganic cores are independent of the matrices, in agreement with the existence of a two-phase system.

As seen above, vdW forces involved at the interphase, play a crucial role, promoting QDs interaction with the polymer chains and/or spontaneous aggregation and, therefore, stimulate the growth of clusters [19]. Thus, the different morphologies when CdTe-DDT QDs are dispersed

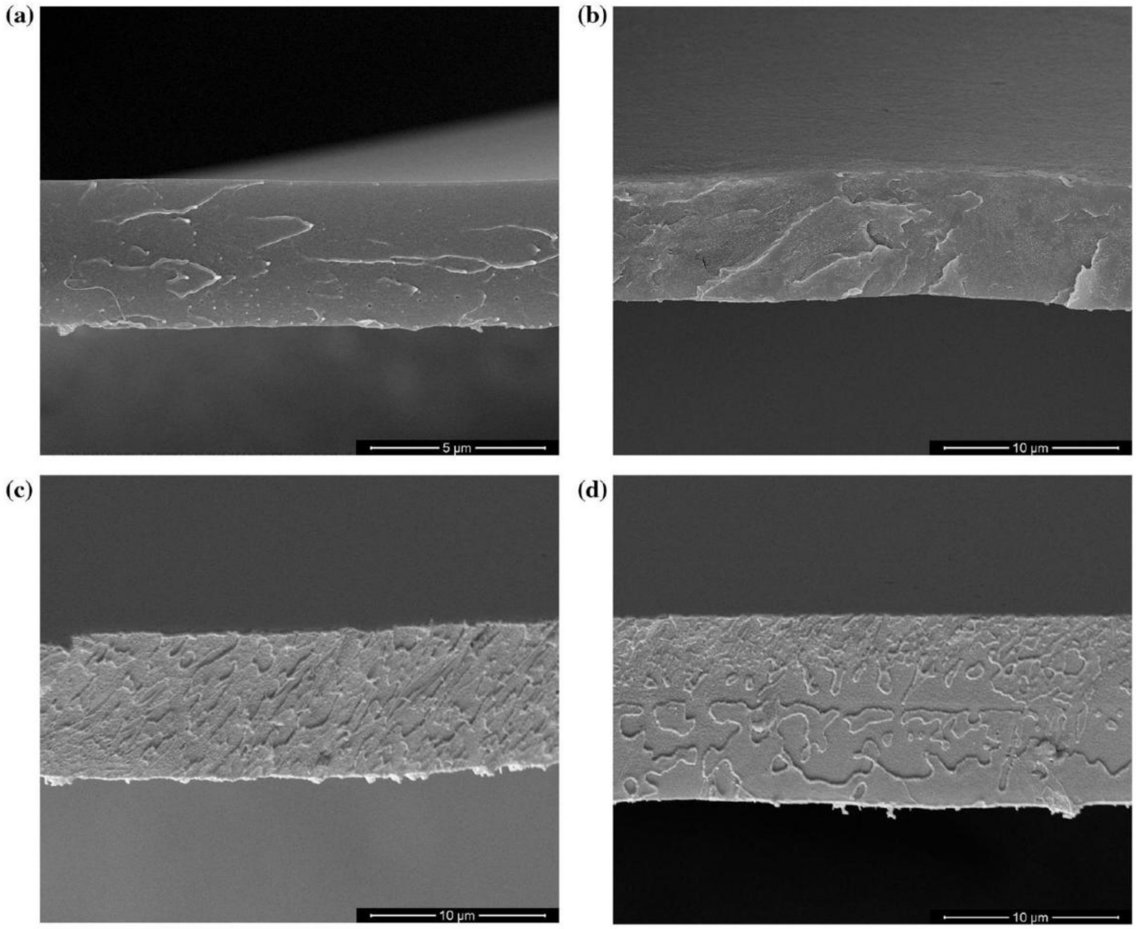

Figure 5 STEM micrographs of PC (a), PMMA (b), PS (c), and OPS (d) thin films obtained upon solvent evaporation at 55°C.
within the polymer matrices used can be explained by vdW along with the polymer chains flexibility.

UV-Visible absorption spectra of the nanocomposites are depicted in Fig. 7a. Compared with the chloroform solution of CdTe-DDT QDs, whose absorption peak position is at approximately 625 nm , a small red-shift in the excitonic peak (~ 627 nm) that support the increase of the nanoparticles size can be noticed [30], as observed by STEM and TEM (Fig. 6). Furthermore, it was observed a spectra broadening of the first electronic transition, which is attributed to the close-packed state of the CdTe QDs in the polymeric matrices [31]. Particularly, for the case of QDs dispersed within PC, the absorption spectrum
displayed a significant decrease of the excitonic peak, which can be associated to the higher particles size or even to the presence of defects on the QDs surface [30]. Along with the evolution of the absorption, it was also observed a red-shift and spectra broadening of the PL emission peaks, with variable intensity, depending on the polymer matrix (Fig. 7b). The bonding of 1-dodecanethiol molecules onto the QDs' surface can induce electrostatic or steric barriers that can compete with vdW forces or depletion interaction [32]. As a result, the aggregation changes the optical properties, with a red-shift. Another possible explanation can be related to the presence of defects on the QDs' surface, caused by the polymers' functional groups. These defects might hinder the direct

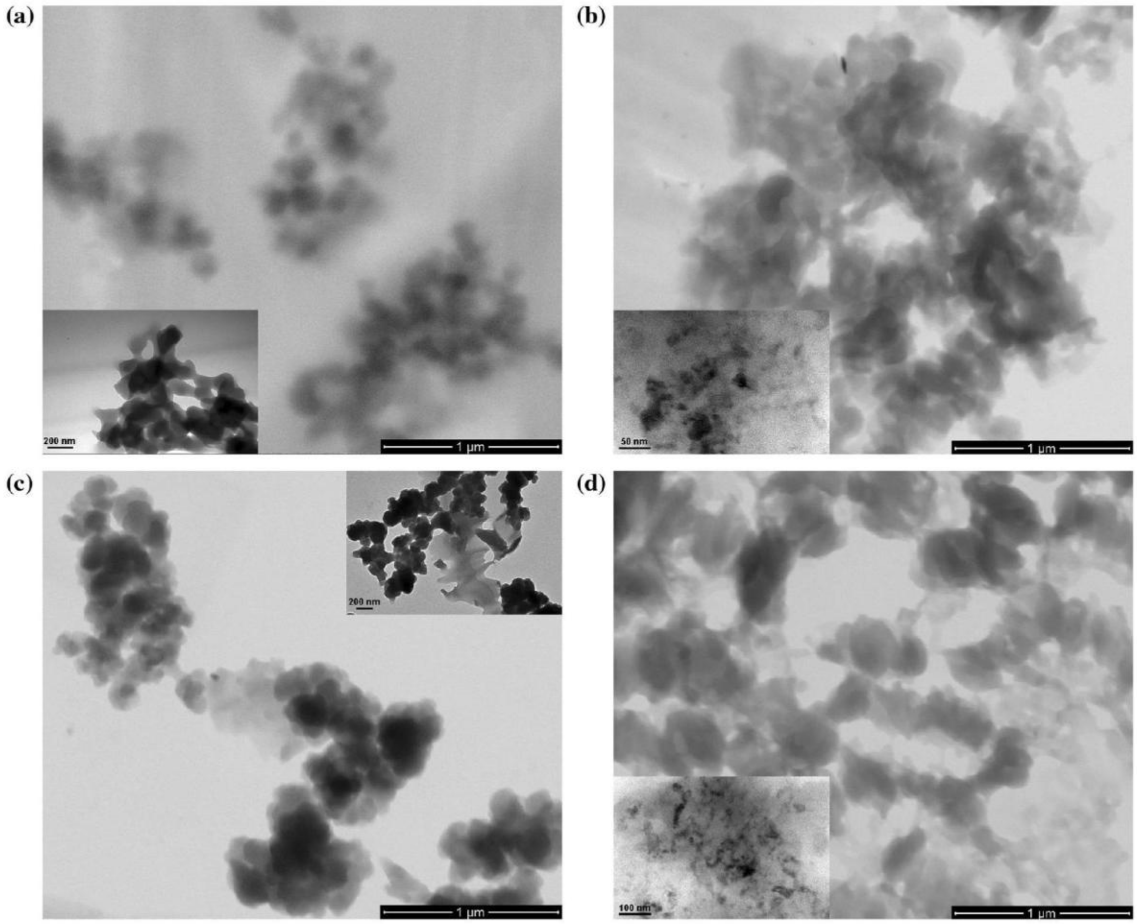

Figure 6 STEM micrographs of CdTe-DDT QDs dispersed in PC (a), PMMA (b), PS (c), and PSO (d). The insets correspond to the TEM micrographs.

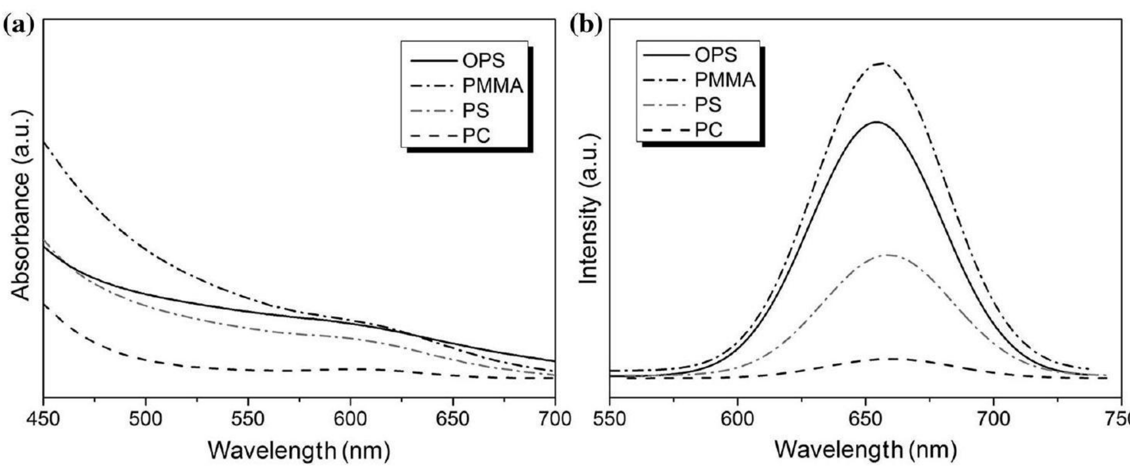

Figure 7 UV-Visible absorption spectra (a) and emission spectra (b) of polymer-QD nanocomposites.

recombination of the excited electrons in the valence band and, therefore, induce a reduction in the emission of photon flux [33]. Usually, either increasing NPs' size or aggregation-induced energy transfer contributes to spectra red-shift [34]. This shift is due to the reabsorption of light emitted from small nanoparticles by the larger ones within the composites. Thus, based on the results showing NPs' aggregation, the observed red-shift can be mainly associated to the increase of NPs' size, with a smaller contribution from the energy transfer. Moreover, QDs dispersed in all polymeric matrices suffered from photoluminescence quenching, especially for PC and PS. One possible explanation could be related with the larger size and aggregation of QDs into these matrices, resulting in the enhancement of dangling bond population on QDs surface, which promotes nonradiative recombination, leading to quenching emission [35].

Electric measurements were performed to evaluate the potential of the solvent casting nanocomposites for optoelectronic applications. From the curves depicted in Fig. 8, it is possible to observe that the PC-based nanocomposite film does not exhibit a detectable photocurrent, evidencing poor charge transport. Nevertheless, for the other nanocomposites (PMMA-, OPS- and PS-based), the current measurements suggested a significant improvement in charge transport, being the film based on PMMA the one that showed highest electric conductivity, under the effect of an electric field. This behavior arises from

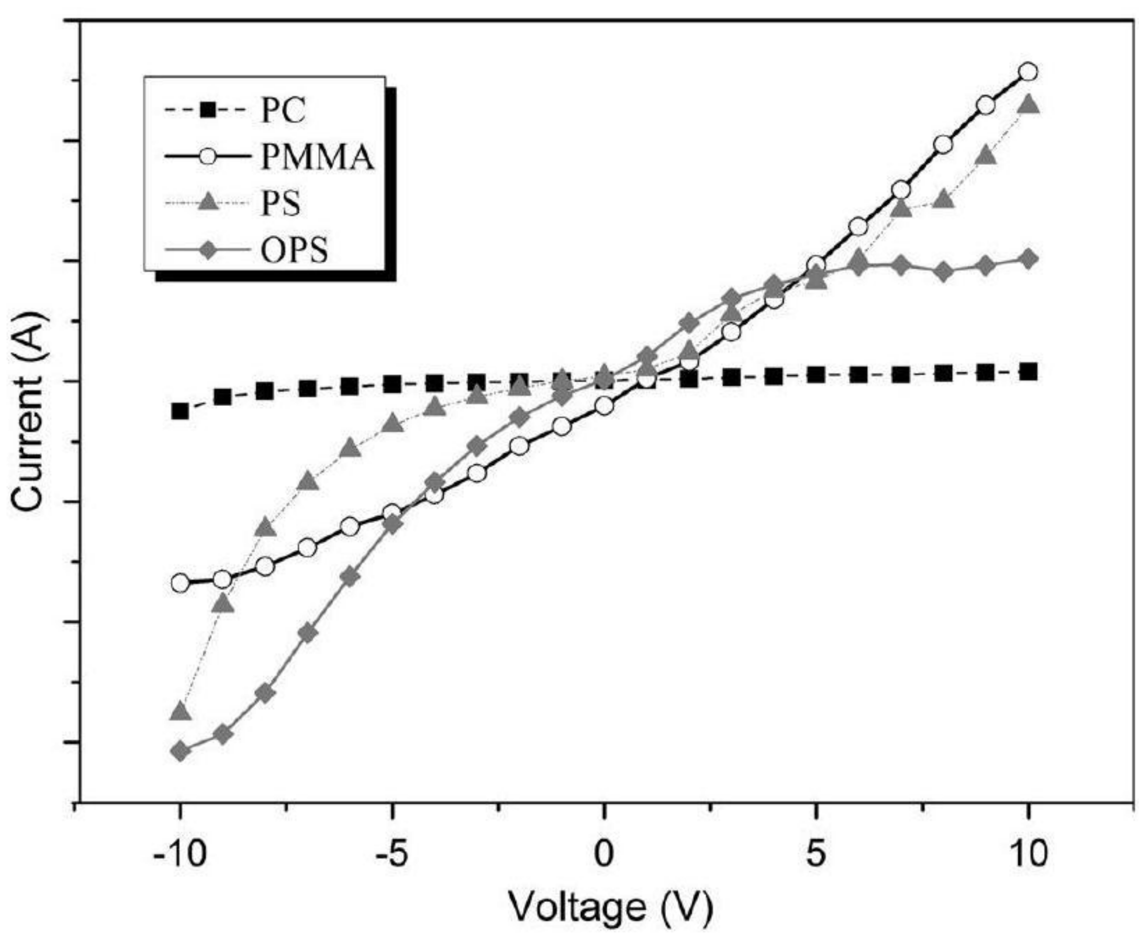

Figure 8 $I-V$ curves of the developed QD-polymer nanocomposites performed at 55°C.

the interconnected QDs network within the thin films, which can be rationalized by the linkage of QDs during the films processing [36]. Accordingly, this proves the efficient incorporation of QDs within the polymer matrix and a strong interaction between PMMA and QDs, which are consistent with the STEM and TEM observations (Fig. 6).

This nanocomposite films contained 13wt% QDs, since this concentration allows an excellent NPs' solubility and is suitable to produce films with good quality, without QDs agglomeration and phase separation. This amount has a great effect on the charge transport of the nanocomposites, since electrical conductivity for the resulting nanocomposites is higher than that of neat polymers. Thus, the presence of QDs allows the conduction mechanism, which lies in the energy gap or act as donor and acceptor sites. It is expected that these sites enable the hopping of electrons between valence and conduction bands and, therefore, enhance the electric conductivity [37].

Another interesting fact, is related with the average roughness (Ra) of the materials, obtained by AFM. As this value increases, the conductivity decreases, suggesting that this parameter has high influence on the electrical properties of the developed materials. The Ra values for PMMA and OPS films were found to be 8 nm and 13 nm , respectively, while for PC and PS-based nanocomposites were higher, 70 nm and 27 nm , respectively. It is well known that surface inhomogeneity's in semiconducting films significantly affect the electric conductivity, due to the scattering centers [38]. Hence, for PC films, which has the highest rough surface (70 nm), the conductivity is reduced, probably due to the boundary filled with nonsemiconducting NPs, confirmed by the existence of large aggregates and therefore, it may give rise to higher electron scattering [38].

Despite the electric conductivity of OPS nanocomposite, PS and PMMA showed a diode-like behavior, being a crucial prerequisite for optoelectronic applications.

Conclusions

Tuneable and highly fluorescent semiconducting CdTe QDs were modified and incorporated into different commercially available polymers using a simple methodology, resulting in quite photoluminescent nanocomposites. The morphology characterization showed that the polymer matrix influences the nanoparticle size and its distribution. Optical absorption and photoluminescence spectroscopy also indicate that the average particle size of CdTe-DDT QDs is lower when embedded in PMMA and OPS matrices. The $I - V$ curves of the developed films showed that they are able to transport charge, thus making them suitable for applications that require conductive materials. The methodology described in this paper allowed to efficiently prepare materials in a simple way, cost-effective, and selective polymer-QD nanocomposites for optoelectronic applications. Additional experiments are being carried out in order to optimize these systems toward the development of materials with improved properties.

Acknowledgements

The authors acknowledge the n-STeP-Nanostructured systems for Tailored Performance, with reference NORTE-07-0124-FEDER-000039, supported by the Programa Operacional Regional do Norte (ON.2), PEst-C/CTM/LA0025/2013 (Strategic Project - LA 25-2013-2014). The authors also acknowledge Agnieszka Tercjak from Dpto. Ingeniería Química y del Medio Ambiente, Escuela Politécnica Donostia-San Sebastián for the AFM measurements.

References

[1] Seo Y-S, Raj CJ, Kim D-J, Kim BC, Yu K-H (2014) Effect of CdS/ZnS quantum dots dispersion in silicone based polymeric Fluids. Mater Lett 130:43-47
[2] Bardajee GR, Hooshyar Z (2013) CdTe quantum dots embedded in a multidentate biopolymer based on salep: characterization and optical properties. J Chem. Article ID 202061
[3] Suárez I, Gordillo H, Abargues R, Albert S, Martínez-Pastor J (2011) Photoluminescence waveguiding in CdSe and CdTe QDs-PMMA nanocomposite films. Nanotechnology 22:435202-435209
[4] Zhu L, Yang S, Wang J, Wang C-F, Chen L, Chen S (2013) Quantum-dot-embedded polymeric fiber films with photoluminescence and superhydrophobicity. Mater Lett 99:54-56
[5] Tomczak N, Janczewski D, Han M, Vancso GJ (2009) Designer polymer-quantum dot architectures. Prog Polym Sci 34(5):393-430
[6] Kim HC, Hong HG, Yoon C, Choi H, Ahn IS, Lee DC, Kim YJ, Lee K (2013) Fabrication of high quantum yield quantum dot/polymer films by enhancing dispersion of quantum dots using silica particles. J Colloid Interface Sci 393:74-79
[7] Ullah MH, Kim J-H, Ha C-S (2008) Highly transparent oPDA functionalized ZnS-polymer nanocomposite thin films with high refractive index. Mater Lett 62(15):2249-2252
[8] Lawrence WG, Thacker S, Palamakumbura S, Riley KJ, Nagarkar VV (2012) Quantum dot-organic polymer composite materials for radiation detection and imaging. IEEE Trans Nucl Sci 59(1):215-221
[9] Zhang H, Tang Y, Zhang J, Li M, Yao X, Li X, Yang B (2009) Manipulation of semiconductor nanocrystals growth in polymer soft materials. Soft Matter 5:4113-4117
[10] Silva FO, Carvalho MS, Mendonça R, Macedo WAA, Balzuweit K, Reiss P, Schiavon MA (2012) Effect of surface ligands on the optical properties of aqueous soluble CdTe Quantum dots. Nanoscale Res Lett 7:536-545
[11] Mansurand HS, Mansur AAP (2011) CdSe quantum dots stabilized by carboxylic-functionalized PVA: synthesis and UV-Vis spectroscopy characterization. Mater Chem Phys 125(3):709-717
[12] Shavel A, Gaponik N, Eychmüller A (2006) Factors governing the quality of aqueous CdTe nanocrystals: calculations and experiment. J Phys Chem B 110(39):19280-19284
[13] Zhang H, Zhou Z, Yang B, Gao M (2003) The influence of carboxyl groups on the photoluminescence of mercaptocarboxylic acid-stabilized CdTe nanoparticles. J Phys Chem B 107(1):8-13
[14] Gaponik N, Talapin DV, Rogach AL, Eychmuller A, Weller H (2002) Efficient phase transfer of luminescent thiol-capped nanocrystals: from water to nonpolar organic solvents. Nanolleters 2(8):803-806
[15] Zhang H, Cui Z, Wang Y, Zhang K, Ji X, Lü C, Yang B, Gao M (2003) From water-soluble cdte nanocrystals to fluorescent nanocrystal-polymer transparent composites using polymerizable surfactants. Adv Mater 15:777-780
[16] Zhang H, Wang C, Li M, Zhang J, Lu G, Yang B (2005) Fluorescent nanocrystal-polymer complexes with flexible processability. Adv Mater 17:853-857
[17] Pang L, Shen Y, Tetz K, Fainma Y (2005) PMMA quantum dots composites fabricated via use of pre-polymerization. Opt Express 13(1):44-49
[18] Ananthakumar S, Ramkumar J, Moorthy Babu S (2013) Enhanced light absorption in CdTe nanoparticles/P3HT nanofiber blends. AIP Conf Proc 1536:167-168
[19] Meli L, Green PF (2008) Aggregation and coarsening of ligand-stabilized gold nanoparticles in poly(methyl methacrylate) thin films. ACS Nano 2:1305-1312

[20] Kane RS, Cohen RE, Silbey R (1999) Semiconductor nanocluster growth within polymer films. Langmuir 15:39-43
[21] Moradian R, Elahi M, Hadizadeh A, Roshani M, Taghizadeh A, Sahraei R (2013) Structural, optical, and electrical properties of thioglycolic acid-capped CdTe quantum dots thin films. Int Nano Lett 3:56-61
[22] Klayman DL, Griffin TS (1973) Reaction of selenium with sodium borohydride in protic solvents. A Facile Method for the introduction of selenium into organic molecules. J Am Chem Soc 95(1):197-199
[23] Gao M, Kirstein S, Möhwald H, Rogach AL, Kornowski A, Eychmüller A, Weller H (1998) Strongly photoluminescent CdTe nanocrystals by proper surface modification. J Phys Chem B 102(43):8360-8363
[24] López F, Ojeda P, Arbeloa I (1989) Fluorescence selfquenching of the molecular forms of Rhodamine B in aqueous and ethanolic solutions. J Luminesc 44:105-112
[25] Stuart BH (2004) Infrared spectroscopy: fundamentals and applications. Wiley, New York
[26] Yu WW, Qu L, Guo W, Peng X (2003) Experimental determination of the extinction coefficient of CdTe, CdSe and CdS nanocrystals. Chem Mater 15:2854-2860
[27] Ananthakumar S, Ramkumar J, Moorthy Babu S (2013) Synthesis and efficient phase transfer of cdse nanoparticles for hybrid solar cell applications. In: Conference papers in energy, vol 2013, p 3
[28] Gopi A, Vindhyasarumi A, Yoosaf K (2015) Electrostatically driven self-assembly of CdTe nanoparticles with organic chromophores probed via Ham effect. RSC Adv 5(59):47813-47819
[29] Gregorio RJ, Ueno EM (1999) Effect of crystalline phase, orientation and temperature on the dielectric properties of poly (vinylidene fluoride) (PVDF). J Mater Sci 34(18):4489-4500
[30] Rajabi HR, Khani O, Shamsipur M, Vatanpour V (2013) High-performance pure and Fe^{3+}-ion doped ZnS quantum dots as green nanophotocatalysts for the removal of malachite green under UV-light irradiation. J Hazard Mater 250-251:370-378
[31] Cao X, Li CM, Bao H, Bao Q, Dong H (2007) Fabrication of strongly fluorescent quantum dot-polymer composite in aqueous solution. Chem Mater 19(15):3773-3779
[32] Yoon C, Hong H-G, Kim HC, Hwang D, Lee DC, Kim C-K, Kim Y-J, Lee K (2013) High luminescence efficiency white light emitting diodes based on surface functionalized quantum dots dispersed in polymer matrices. Colloids Surf A 428:86-91
[33] Thuy UTD, Liem NQ (2013) Transition from type-I to typeII CdTe/CdS core/shell quantum dots synthesized in water at low temperature. Adv Nat Sci 4(4):045010-045015
[34] Tang Z, Kotov NA, Giersig M (2002) Spontaneous organization of single CdTe nanoparticles into luminescent nanowires. Science 297(5579):237-240
[35] Jakubiak R, Collison CJ, Wan WC, Rothberg LJ, Hsieh BR (1999) Aggregation quenching of luminescence in electroluminescent conjugated polymers. J Phys Chem A 103(14):2394-2398
[36] Korala L, Wang Z, Liu Y, Maldonado S, Brock SL (2013) Uniform thin films of CdSe and CdSe(ZnS) core(shell) quantum dots by sol-gel assembly: enabling photoelectrochemical characterization and electronic applications. ACS Nano 7(2):1215-1223
[37] Ranjbartoreh AR, Ghorbanpour A, Soltani B (2007) Doublewalled carbon nanotube with surrounding elastic medium under axial pressure. Physica E 39(2):230-239
[38] Ketenoğlu D, Ünal B (2013) Influence of surface roughness on the electrical conductivity of semiconducting thin films. Physica A 392(14):3008-3017